

Outage Probability Analysis of THz Relaying Systems

Alexandros–Apostolos A. Boulogeorgos, and Angeliki Alexiou
 Department of Digital Systems, University of Piraeus, Piraeus, Greece
 E-mails: al.boulogeorgos@ieee.org, alexiou@unipi.gr

Abstract—This paper focuses on quantifying the outage performance of terahertz (THz) relaying systems. In this direction, novel closed-form expressions for the outage probability of a dual-hop relaying systems, in which both the source-relay and relay-destination links suffer from fading and stochastic beam misalignment, are extracted. Our results reveal the importance of taking into account the impact of beam misalignment when characterizing the outage performance of the system as well as when selecting the transmission frequencies.

Index Terms—THz wireless systems, Outage probability, Performance analysis.

I. INTRODUCTION

Despite the adaptation of several game changing technologies, the envelop of fifth generation (5G) systems capabilities has been proven to be defined by the available bandwidth [1]–[5]. Motivated by this, next generation networks are expected to exploit higher frequency bands, such as the terahertz (THz) one [6]–[10]. However, THz links experience high channel attenuation, which significantly limits the communication range [11]–[14].

To overcome the aforementioned limitation, researchers have recently turned their attention to relaying systems [15]–[19]. In more detail, in [15] and [16], the authors used Monte Carlo simulations in order to quantify the outage performance of a relay-assisted in-vivo nano-scale network in the absence and presence of direct link that operates in the THz band. For the same system model, in [17], the energy efficiency was evaluated. Additionally, in [18], a number of different relaying strategies for macro-scale THz systems was discussed. Finally, in [19], the outage and error performance of a mixed microwave-THz wireless systems were assessed.

To the best of the author’s knowledge, the theoretical framework for the evaluation of THz wireless relaying systems performance remains vastly unexplored. Motivated by this, this paper studies the outage performance of such systems. In particular, we extract novel closed-form expressions for the system outage probability (OP), which reveal the joint impact of beam misalignment (BM), and multi-path fading.

This work has received funding from the European Commission’s Horizon 2020 research and innovation programme under grant agreement No. 761794.

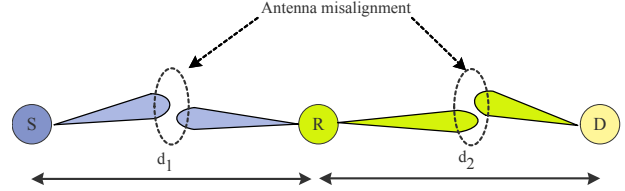


Fig. 1: System model.

Notations: The operator $|\cdot|$ denotes the absolute value, whereas $\exp(x)$ represents the exponential function. Additionally, \sqrt{x} returns the square root of x , while, $\min(\cdot)$ stands for the minimum operator. Meanwhile, the set of the complex numbers is represented by \mathbb{C} . In addition, $P_r(\mathcal{A})$ represents the probability that the event \mathcal{A} is valid. Finally, the upper and lower incomplete Gamma functions [20, eq. (8.350/2), (8.350/3)] are respectively denoted by $\Gamma(\cdot, \cdot)$ and $\gamma(\cdot, \cdot)$, while the Gamma function is represented by $\Gamma(\cdot)$ [20, eq. (8.310)].

II. SYSTEM MODEL

As illustrated in Fig. 1, we consider a dual-hop decode-and-forward (DF) relaying system, in which all nodes operate in the THz band. The source (S), relay (R), and destination (D) nodes are respectively equipped with N_s , N_r , and N_d antenna elements, and support analog beamforming. Moreover, it is assumed that there is no direct link between S and D. Finally, we assume that R operates in half-duplex mode. As a result, each communication period is divided into two phases. In the first one, S transmits to R, while, in the second one, R decodes, re-encodes and re-transmits the received signal to D. In what follows, for the sake of simplicity, we refer to the S-R and R-D links as the 1–st and 2–nd one, respectively.

During the first phase, the baseband equivalent received signal at R can be expressed as

$$y_r = \mathbf{u}_r^* \mathbf{H}_r \mathbf{v}_s s + n_r, \quad (1)$$

where n_r is the adaptive white Gaussian noise (AWGN) with variance $N_{o,1}$, while \mathbf{u}_r^* and \mathbf{v}_s respectively represent the R and S beamforming vectors. Likewise, s stands for the S transmitted signal, while \mathbf{H}_r is the complex MIMO channel matrix.

Similarly, in the end of the second phase, the baseband equivalent received signal at R can be obtained as

$$y_d = \mathbf{u}_d^* \mathbf{H}_d \mathbf{v}_r \tilde{s} + n_d, \quad (2)$$

with n_d being the AWGN with variance $N_{o,2}$, whereas \mathbf{u}_d^* and \mathbf{v}_r respectively represent the D and R beamforming vectors. Finally, \tilde{s} stand for the re-transmitted by D signal.

The MIMO channel matrix \mathbf{H}_i with $i \in \{1, 2\}$ can be modeled as

$$\mathbf{H}_i = h_i \mathbf{u}_i \mathbf{v}_i^*, \quad (3)$$

where \mathbf{u}_1 and \mathbf{v}_1 are the R and S perfectly-aligned beamspace directions for the S-R link, while \mathbf{u}_2 and \mathbf{v}_2 stands for the corresponding vectors of the R-D link. Finally, h_i stands for the i -th channel coefficient and can be analytically obtained as

$$h_i = h_i^{(l)} h_i^{(f)} h_i^{(m)}. \quad (4)$$

In (4), $h_i^{(l)}$ stands for the deterministic path gain coefficient and can be obtained as [21, eqs. (5)-(17)]

$$h_i^{(l)} = \begin{cases} \frac{c\sqrt{G_s G_{r,r}}}{4\pi f_1 d_1} \exp\left(-\frac{1}{2}\beta(f_1) d_1\right), & \text{for } i = 1 \\ \frac{c\sqrt{G_{r,t} G_d}}{4\pi f_2 d_2} \exp\left(-\frac{1}{2}\beta(f_2) d_2\right), & \text{for } i = 2 \end{cases}, \quad (5)$$

where c and β respectively stand for the speed of light and the molecular absorption coefficient, while G_s , $G_{r,t}$, $G_{r,r}$, and G_d are the source, relay transmission and reception, and destination antenna gains, respectively. Likewise, f_i and d_i with $i \in \{1, 2\}$ are the transmission frequency and distance of the S-R and R-D links. Note that in the 275 – 425 GHz range, the molecular absorption coefficient can be accurately evaluated as [22]

$$\beta(f_i) = \sum_{k=1}^3 u_k(f_i), \quad \text{with } i \in \{1, 2\}, \quad (6)$$

where

$$u_k(f_i) = \begin{cases} \frac{A_k}{B_k + \left(\frac{f_i}{c} - \delta_k\right)}, & \text{for } k \in \{1, 2\} \\ \sum_{l=0}^3 p_l f^l, & \text{for } k = 3 \end{cases}, \quad (7)$$

with

$$A_k = \begin{cases} g_1 v (g_2 v + g_3), & \text{for } k = 1 \\ g_4 v (g_5 v + g_6), & \text{for } k = 2 \end{cases}, \quad (8)$$

and

$$B_k = \begin{cases} (g_7 v + g_8)^2, & \text{for } k = 1 \\ (g_9 v + g_{10})^2, & \text{for } k = 2 \end{cases}, \quad (9)$$

In (7), $\delta_1 = 10.835 \text{ cm}^{-1}$, $\delta_2 = 12.664 \text{ cm}^{-1}$, $p_0 = -6.36 \times 10^{-3}$, $p_1 = 9.06 \times 10^{-14} \text{ s}$, $p_2 = -3.94 \times 10^{-25} \text{ s}^2$, $p_3 = 5.54 \times 10^{-37} \text{ s}^3$. Meanwhile, in (8) and (9), $g_1 = 0.2205$, $g_2 = 0.1303$, $g_3 = 0.0294$, $g_4 = 2.014$, $g_5 = 0.1702$, $g_6 = 0.0303$, $g_7 = 0.4093$, $g_8 = 0.0925$, $g_9 = 0.537$, and $g_{10} = 0.0956$. Finally,

v represents the volume of mixing ratio of the water vapor and can be obtained as $v = \phi \frac{p_s(T, p_h)}{p_h}$, where p_s and p_h are respectively the relative humidity and the atmospheric pressure in hPa. Finally, $p_s(T, p_h)$ represents the saturated water vapor partial pressure in temperature T and atmospheric pressure p_h , and can be expressed as $p_s(T, p_h) = \kappa_1 (\kappa_2 + \kappa_3 p_h) \exp\left(\kappa_4 \frac{T - \kappa_5}{T - \kappa_6}\right)$, where $\kappa_1 = 6.1121 \text{ hPa}$, $\kappa_2 = 1.0007$, $\kappa_3 = 3.46 \times 10^{-6} \text{ hPa}^{-1}$, $\kappa_4 = 17.502$, $\kappa_5 = 273.15 \text{ }^\circ\text{K}$, and $\kappa_6 = 32.18 \text{ }^\circ\text{K}$.

Moreover, h_i^f represents the fading coefficient. Note that the envelop of $h_i^{(f)}$ is assumed to follow a generalized Gamma distribution with probability density function (PDF) and cumulative density function (CDF) that can be respectively expressed as

$$f_{|h_i^{(f)}|}(x) = \frac{\alpha_i \mu_i^{\alpha_i} x^{\alpha_i \mu_i - 1}}{\left(\hat{h}_i^{(f)}\right)^{\alpha_i \mu_i} \Gamma(\mu_i)} \exp\left(-\mu_i \frac{x^{\alpha_i}}{\left(\hat{h}_i^{(f)}\right)^{\alpha_i}}\right) \quad (10)$$

and

$$F_{|h_i^{(f)}|}(x) = 1 - \frac{\Gamma\left(\mu_i, \mu_i \frac{x^{\alpha_i}}{\left(\hat{h}_i^{(f)}\right)^{\alpha_i}}\right)}{\Gamma(\mu_i)}, \quad (11)$$

where $\alpha_i > 0$ is a fading parameter, μ_i is the normalized variance of the fading channel envelope, and $\hat{h}_i^{(f)}$ is the α_i -root mean value of the fading channel envelop. Additionally, $h_i^{(m)}$ stands for the misalignment fading coefficient and its PDF can be obtained as $f_{h_i^{(m)}}(x) = \frac{\zeta_i}{S_{o,i}^{\zeta_i}} x^{\zeta_i - 1}$, $0 \leq x \leq S_{o,i}$, where $S_{o,i}$ is the portion of the collected signal at the receiver of the i -th link under perfect alignment conditions, whereas $\zeta = \frac{w_i^2}{4\sigma_{s,i}^2}$ with w_i and $\sigma_{s,i}$ respectively being the equivalent beam-width and jitter standard deviation at the receiver plane of the i -th link.

Finally, by assuming that, during the initial access phase, the optimal beamforming vectors have been selected; hence, the beam directions are orthogonal, i.e., $\mathbf{u}_{r,1}^* \mathbf{u}_1 \mathbf{v}_1^* \mathbf{v}_{s,1} = 1$, and $\mathbf{u}_{d,2}^* \mathbf{u}_2 \mathbf{v}_2^* \mathbf{v}_{r,2} = 1$, and that the BM can be fully modeled by $h_i^{(m)}$, $i \in \{1, 2\}$, with the aid of (3), (1) and (2) can be respectively simplified as

$$y_r = h_1 s + n_r \quad (12)$$

and

$$y_d = h_2 \tilde{s} + n_d. \quad (13)$$

III. PERFORMANCE ANALYSIS

A. End-to-end SNR statistics

Since R operates in DF mode, the equivalent end-to-end SNR can be obtained as

$$\rho_e = \min(\rho_1, \rho_2), \quad (14)$$

where ρ_1 and ρ_2 are respectively the S-R and R-D link SNRs and can be obtained as

$$\rho_i = \bar{\rho}_i |h_i^{(fm)}|^2, \quad (15)$$

with $i \in \{1, 2\}$, $|h_i^{(fm)}|^2 = |h_i^{(f)}|^2 |h_i^{(m)}|^2$, and P_1, P_2 respectively being the S and R transmitted powers.

The following theorem and lemmas return the CDF of ρ_e for the general case in which both S-R and R-D links experience BM, as well as for the special cases in which a single or no link suffers for BM.

Theorem 1. *For the general case, in which both links suffer from BM, the CDF of ρ_e can be evaluated as*

$$F_{\rho_e}(x) = 1 - \prod_{i=1}^2 \sum_{k=0}^{\mu_i-1} \frac{x^{\zeta_i/2}}{\alpha_i \bar{\rho}_i^{\zeta_i/2} \left(\hat{h}_i^{(f)}\right)^{\zeta_i} \frac{\zeta_i}{S_{o,i}^{\zeta_i}} \frac{\mu_i^{\zeta_i}}{k!}} \times \Gamma\left(\frac{\alpha_i k - \zeta_i}{\alpha_i}, \frac{\mu_i S_{o,i}^{-\alpha_i} x^{\alpha_i/2}}{\bar{\rho}_i^{\alpha_i/2} \left(\hat{h}_i^{(f)}\right)^{\alpha_i}}\right). \quad (16)$$

Proof: Please refer to Appendix A. ■

Lemma 1. *For the special case in which only one of the S-R and R-D links suffer from BM, the CDF of the end-to-end equivalent SNR can be expressed as (17), given at the top of the next page.*

Proof: Please refer to Appendix B. ■

Lemma 2. *For the case in which no-link experience BM, the end-to-end equivalent SNR can be written as*

$$F_{\rho_j^{\text{id}}}(x) = 1 - \prod_{j=1}^2 \frac{\Gamma\left(\mu_j, \mu_j \frac{x^{\alpha_j/2}}{\left(\hat{h}_j^{(f)}\right)^{\alpha_j} \bar{\rho}_j^{\alpha_j/2}}\right)}{\Gamma(\mu_j)}. \quad (18)$$

Proof: Please refer to Appendix C. ■

B. Outage Analysis

The OP of the equivalent e2e link can be defined as the probability that the equivalent e2e SNR falls below a predetermined threshold, ρ_{th} , i.e. $P_o = P_r(\rho_e \leq \rho_{th})$, or equivalently

$$P_o = \begin{cases} F_{\rho_e}(\rho_{th}), & \text{both links suffer from BM} \\ F_{\rho_e}^{sc}(\rho_{th}) & \text{only one link suffers from BM} \\ F_{\rho_j^{\text{id}}}(\rho_{th}) & \text{no link suffers from BM} \end{cases}. \quad (19)$$

IV. RESULTS & DISCUSSION

Respective numerical results for different scenarios are presented in this section to highlight the joint effect of antenna misalignment and fading. In more detail, the following insightful scenario is considered. The THz relaying system is operating under standard environmental conditions, i.e. the relative humidity is 50%, the atmospheric pressure equals 101325 Pa and

the temperature is set to 296°K. Moreover, the operation frequency is 275 GHz, the transmit and receive antenna gains of both the S and R are set to 55 dBi. The S-R and R-D links transmission distances are set to 10 m. Finally, unless otherwise stated, $\alpha_1 = \alpha_2 = 1$, and $\mu_1 = \mu_2 = 3$. It should be noted that each of the following figures contains both analytical and Monte Carlo results represented by lines and discrete marks, respectively.

Figure 2 demonstrates the outage performance of the relaying systems for different values of f_1, f_2 and BM scenarios. In more detail, in Fig. 2.a, the OP is plotted against f_1 and f_2 , assuming that both the S-R and R-D links experience the same levels of BM, i.e. $\sigma_{s,1} = \sigma_{s,2} = 1$ cm. Similarly, the outage performance for the case in which only the S-R link experience BM of $\sigma_{s,1} = 1$ cm, while the R-D one is BM-free is plotted in Fig. 2.b, whereas the case in which the R-D link suffers from BM of $\sigma_{s,2} = 1$ cm and the S-R is BM-free is provided in Fig. 2.c. As a benchmark, in Fig. 2.d, the OP performance of the BM-free relaying system are depicted. For the shake of comparison, in Fig. 2.e, the OP is plotted as a function of f_1 , for $f_2 = 275$ GHz and 383 GHz, which are respectively the best and worst case scenario, and for all the aforementioned BM scenarios. From Fig. 2.a, it becomes evident that, for the case in which both links suffer from BM, there exist a low OP transmission windows for $f_1, f_2 \in [275, 320]$ GHz]. Moreover, the worst outage performance are met for $f_1 = f_2 = 383$ GHz. From Figs. 2.b and 2.c, it is observed that, for a fixed OP requirement, the link that suffers from BM determines the bandwidth of the transmission signal. Moreover, from Fig. 2.d, it is revealed that even in the absence of BM, the best and worst outage performance are respectively met for $f_1 = f_2 = 275$ GHz and $f_1 = f_2 = 383$ GHz, where the minimum and maximum path-loss is observed. This indicates the detrimental impact of path-loss on the system performance. Likewise, from Fig. 2.e, it becomes evident that, for a given f_1 , as f_2 increases, the OP also increases. Also, for a fixed f_2 , as f_1 increases, the outage performance degrades. Finally, from this figure, it becomes apparent that the joint impact of BM and path-gain should be taken into account when characterizing the outage performance of the THz relaying system.

Figure 3 illustrates the OP as a function of G_s for different values of $G_{r,r}$ and BM scenarios, assuming $P_1/N_0/\rho_{th} = P_2/N_0/\rho_{th} = 50$ dB, $G_{r,t} = 50$ dBi, and $\sigma_{s,1} = \sigma_{s,2} = 1$ cm. As expected, for given $G_{r,r}$ and BM scenario, as G_s increases, the deterministic path-gain increases and as a consequence the OP decreases. For example, for the case in which both links suffer from BM and $G_{r,r} = 40$ dBi, as G_s shifts from 30 to 50 dBi, the OP decreases for about 30 times. Similarly, we observe that, for fixed G_s and BM scenario,

$$F_{\rho_e}^{sc}(x) = 1 - \sum_{k=0}^{\mu_i-1} \frac{x^{\zeta_i/2}}{\alpha_i \bar{\rho}_i^{\zeta_i/2} (\hat{h}_i(f))} \frac{\zeta_i}{S_{o,i}^{\zeta_i}} \frac{\mu_i^{\zeta_i}}{k!} \Gamma \left(\frac{\alpha_i k - \zeta_i}{\alpha_i}, \frac{\mu_i S_{o,i}^{-\alpha_i} x^{\alpha_i/2}}{\bar{\rho}_i^{\alpha_i/2} (\hat{h}_i(f))^{\alpha_i}} \right) \frac{1}{\Gamma(\mu_j)} \Gamma \left(\mu_j, \mu_j \frac{x^{\alpha_j/2}}{(\hat{h}_i(f))^{\alpha_i} \bar{\rho}_j^{\alpha_j/2}} \right) \quad (17)$$

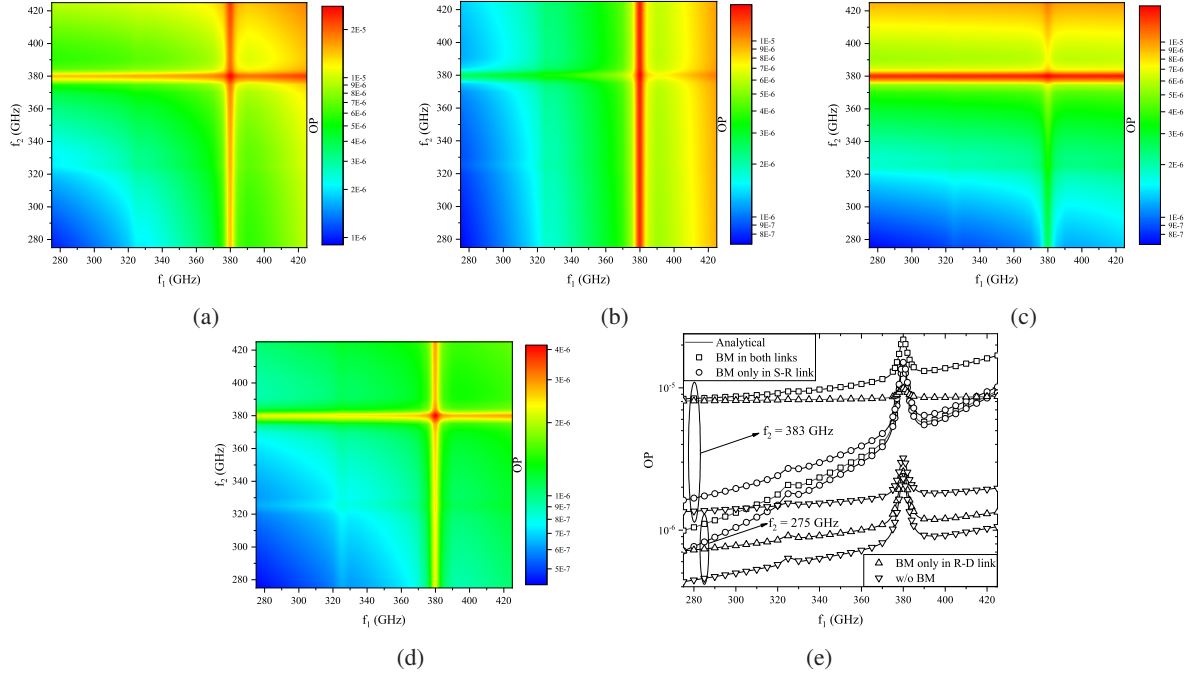


Fig. 2: OP vs f_1 and f_2 , for different the following BM scenarios: (a) both S-R and R-D links experience BM; (b) only S-R link suffers from BM, while R-D is BM-free; (c) only R-D link suffers from BM, while S-R is BM-free; and (d) both S-R and R-D are BM-free. Also, OP vs f_1 for different values od f_2 and all the aforementioned scenarios (e).

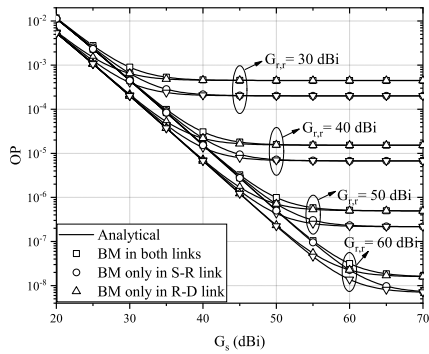


Fig. 3: OP vs G_s , for different values of $G_{r,r}$ and BM scenarios.

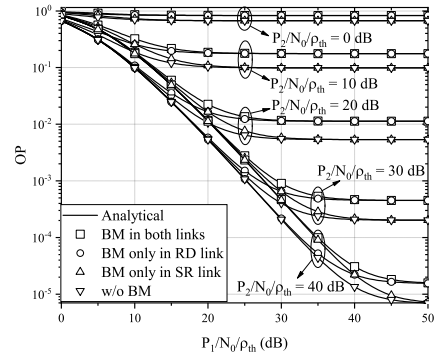


Fig. 4: OP vs $P_1/N_0/\rho_{th}$, for different values of $P_2/N_0/\rho_{th}$ and BM scenarios.

as $G_{r,r}$ increases, the OP decreases. For instance, for the scenario in which both links experience BM and $G_s = 40$ dBi, as $G_{r,r}$ moves from 30 to 50 dBi, the OP decreases approximately 30 times. By comparing, the aforementioned examples, the reciprocity of the link

is revealed. Additionally, from this figure, we observe that there exist a floor on the OP in respect to G_s .

Figure 4 depicts the OP as a function of $P_1/N_0/\rho_{th}$ for different values of $P_2/N_0/\rho_{th}$ and BM scenarios, assuming that $\sigma_{s,1} = \sigma_{s,2} = 1$ cm. In more detail,

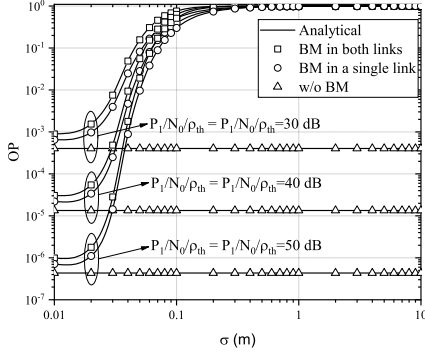


Fig. 5: OP vs σ , for different values of $P_1/N_0/\rho_{th} = P_2/N_0/\rho_{th}$ and BM scenarios.

the following BM scenarios are examined: (i) both links suffer from the same level of BM, (ii) only the SR link experience BM, while RD is BM-free, and (iii) only the R-D link experience BM, while S-R is BM-free. Finally, as a benchmark, the OP for the ideal case, in which both the S-R and R-D links are BM-free, is delivered. From this figure, we observe that, for a fixed $P_2/N_0/\rho_{th}$ and BM scenario, as $P_1/N_0/\rho_{th}$ increases, the OP decreases. For example, for the case in which both links suffer for BM and $P_2/N_0/\rho_{th} = 30$ dB, as $P_1/N_0/\rho_{th}$ increases from 20 to 30 dB, the outage performance improves for about 10 times. Moreover, it becomes apparent that for $P_1/N_0/\rho_{th} \geq P_2/N_0/\rho_{th}$, there exists an OP floor that depends on the quality of the RD link. As a result, in the $P_1/N_0/\rho_{th} \geq P_2/N_0/\rho_{th}$ regime, systems in which only the R-D link suffers from BM, and the corresponding ones that experience BM in both the S-R and R-D links have approximately the same performance, whereas, the same occurs for systems in which only the S-R link suffers from BM and systems that both links are BM-free. Additionally, for a given $P_1/N_0/\rho_{th}$, as $P_2/N_0/\rho_{th}$ increases, the outage performance improves. For instance, for the case in which both links suffer from BM and $P_1/N_0/\rho_{th} = 20$ dB, a $P_2/N_0/\rho_{th}$ increase from 10 to 20 dB results at more than 10 times OP decrease. A similar outage performance improvement also occurs for the cases in which only one or no-link suffers from BM, under the same $P_2/N_0/\rho_{th}$ shift. Finally, we observe that there exist an important performance difference between THz relaying systems that suffer from BM and the corresponding ideal ones. For example, for $P_1/N_0/\rho_{th} = 35$ dB and $P_2/N_0/\rho_{th} = 30$ dB, the system in which only the R-D link suffers from BM achieves 9% better outage performance in comparison with the one that both links experience BM and about 50% worst performance than the one that BM exists in the SR link. This indicates the importance of accurately modeling BM in THz relaying systems.

Figure 5 illustrates the OP as a function of $\sigma_{s,1} = \sigma_{s,2} = \sigma$, for different values of $P_1/N_0/\rho_{th} =$

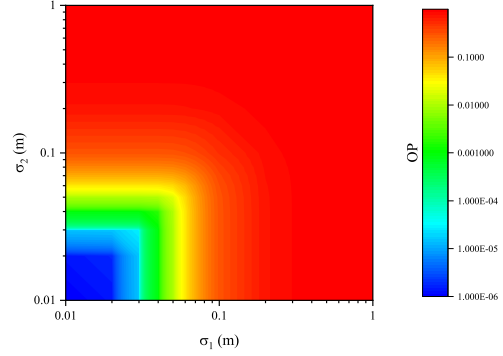


Fig. 6: OP vs σ_1 and σ_2 .

$P_2/N_0/\rho_{th}$ and the following BM scenarios: (i) both the S-R and R-D links suffer from the same level of BM, (ii) either the S-R or the R-D link experience BM, and (iii) both links are BM-free. As expected, for a given $P_1/N_0/\rho_{th} = P_2/N_0/\rho_{th}$, as σ increases, the OP also increases. For example, for $P_1/N_0/\rho_{th} = P_2/N_0/\rho_{th} = 50$ dB and the case in which both links suffer from BM, as σ increases from 1 to 5 cm, the OP also increases from 9.9×10^{-7} to 1.9×10^{-2} . Additionally, for a given σ and BM scenario, as $P_1/N_0/\rho_{th} = P_2/N_0/\rho_{th}$ increases, the outage performance improves. For instance, for $\sigma = 5$ cm, in the case in which both links experience BM, the OP decreases from 5.6×10^{-2} to 1.9×10^{-2} , as $P_1/N_0/\rho_{th} = P_2/N_0/\rho_{th}$ shifts from 40 to 50 dB. Similarly, for the case in which only one link suffers from BM, the same σ and $P_1/N_0/\rho_{th} = P_2/N_0/\rho_{th}$ increase results to an OP increase from 2.8×10^{-2} to 9.69×10^{-3} . Likewise, from this figure, it becomes evident that THz relaying systems in which only one link suffers from BM outperforms the ones that both links experience BM, for the same levels of BM and $P_1/N_0/\rho_{th} = P_2/N_0/\rho_{th}$. Finally, the BM-free THz relaying system outperforms both the aforementioned scenarios.

Figure 6 plots the OP as a function of σ_1 and σ_2 , assuming $P_1/N_0/\rho_{th} = P_2/N_0/\rho_{th} = 50$ dB. As expected, for a fixed σ_1 , as σ_2 increases, the quality of the R-D link degrades; hence, the OP increases. For instance, for $\sigma_1 = 5$ cm, as σ_2 shifts from 1 to 5 cm, the OP changes from 9.69×10^{-3} to 1.93×10^{-2} . Similarly, for a fixed σ_2 , as σ_1 increases, an outage performance degradation occurs. For example, for $\sigma_2 = 2$ cm, as σ_1 increases from 1 to 5 cm, the OP also increases for about ten times.

In Fig. 7, the OP is plotted as a function of G_s , for different values of σ_s , assuming $P_1/N_0/\rho_{th} = P_2/N_0/\rho_{th} = 50$ dB, $\sigma_{s,1} = \sigma_{s,2} = \sigma_s$ and that both links suffer from BM. As a benchmark, the case in which both links are BM-free is also plotted. As expected, for a given σ_s , as G_s increases, the OP decreases. Moreover, for a fixed G_s , as σ_s increases, the outage performance degrades. Finally, an OP floor in the high G_s regime is

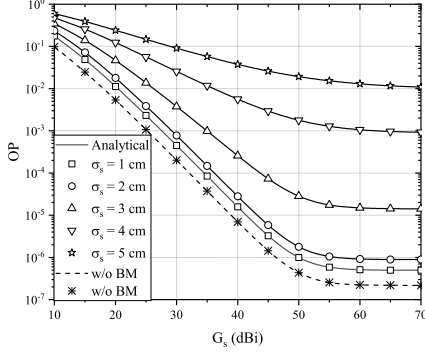


Fig. 7: OP vs G_s , for different values of σ_s .

observed.

V. CONCLUSIONS

In this paper, we presented novel closed-form expressions for the OP of THz wireless relaying systems, which take into account the intermediate links particularities, namely deterministic path-loss, stochastic BM, and fading. Our results highlighted the importance of accurate characterization of the intermediate channels, when assessing and designing such systems.

APPENDICES

VI. APPENDIX A

In general, the CDF of ρ_e can be evaluated as $F_{\rho_e}(x) = \Pr(\rho_e \leq x)$, which, by employing (14), can be rewritten as

$$F_{\rho_e}(x) = \Pr(\min(\rho_1, \rho_2) \leq x), \quad (20)$$

or equivalently

$$F_{\rho_e}(x) = 1 - \Pr(\min(\rho_1, \rho_2) \geq x). \quad (21)$$

The event $\mathcal{U}_1 = \{\min(\rho_1, \rho_2) \geq x\}$ can be rewritten as $\mathcal{U}_1 = \{\rho_1 \geq x\} \cap \{\rho_2 \geq x\}$. Moreover, since $|h_1|$ and $|h_2|$ are independent random variables (RVs), ρ_1 and ρ_2 are also independent RVs; hence, (21) can be simplified as

$$F_{\rho_e}(x) = 1 - \Pr(\{\rho_1 \geq x\}) \Pr(\{\rho_2 \geq x\}), \quad (22)$$

or equivalently

$$F_{\rho_e}(x) = 1 - (1 - \Pr(\{\rho_1 \leq x\}))(1 - \Pr(\{\rho_2 \leq x\})). \quad (23)$$

By taking into account that $\Pr(\{\rho_i \leq x\}) = F_{\rho_i}(x)$ with $i \in \{1, 2\}$, (23) can be expressed as

$$F_{\rho_e}(x) = 1 - \prod_{i=1}^2 (1 - F_{\rho_i}(x)). \quad (24)$$

Next, by employing [21, Eq. (43)] and after some algebraic manipulations, we can rewrite (24) as (16). This concludes the proof.

APPENDIX B

In the special case, in which either the S-R or the R-D link experience BM, according to (24), the CDF of ρ_e can be obtained as

$$F_{\rho_e}^{sc} = (1 - F_{\rho_i}(x)) (1 - F_{\rho_j^{wm}}(x)), \quad (25)$$

where $i, j \in \{1, 2\}$ with $i \neq j$. Note that in (25), $F_{\rho_i}(x)$ denotes the CDF of the SNR of the link that suffers from BM, while $F_{\rho_j^{wm}}(x)$ is the one of the BM-free link.

Next, we derive $F_{\rho_j^{wm}}(x)$ as

$$F_{\rho_j^{wm}}(x) = \Pr(\rho_j^{wm} \leq x), \quad (26)$$

where ρ_j^{wm} is the SNR of the misalignment-free link, which can be expressed as

$$\rho_j^{wm} = \bar{\rho}_i |h_i^{(f)}|^2. \quad (27)$$

From (27), (26) can be rewritten as

$$F_{\rho_j^{wm}}(x) = \Pr\left(|h_i^{(f)}| \leq \sqrt{\frac{x}{\bar{\rho}_i}}\right), \quad (28)$$

or equivalently

$$F_{\rho_j^{wm}}(x) = F_{|h_i^{(f)}|}\left(\sqrt{\frac{x}{\bar{\rho}_i}}\right). \quad (29)$$

By taking into account (11), (29), and [21, Eq. (43)], we can express (25) as (17). This concludes the proof.

APPENDIX C

Following the same steps as Appendix A, the CDF of the end-to-end SNR in the absence of BM in both the S-R and R-D links can be obtained as $F_{\rho_e^{id}}(x) = 1 - \prod_{j=1}^2 (1 - F_{\rho_j^{wm}}(x))$, which, by employing (28), we obtain (18). This concludes the proof.

REFERENCES

- [1] J. Andrews and A. Gatherer, "Will densification be the death of 5G," *ComSoc Technology News*, May 2015.
- [2] A.-A. A. Boulogeorgos, A. Alexiou, D. Kritharidis, A. Katsiotis, G. Ntouni, J. Kokkonen, J. Lethomaki, M. Juntti, D. Yankova, A. Mokhtar, J.-C. Point, J. Machodo, R. Elschner, C. Schubert, T. Merkle, R. Ferreira, F. Rodrigues, and J. Lima, "Wireless terahertz system architectures for networks beyond 5G," *TER-RANOVA CONSORTIUM*, White paper 1.0, Jul. 2018.
- [3] A.-A. A. Boulogeorgos and G. K. Karagiannidis, "Low-cost cognitive radios against spectrum scarcity," *IEEE Technical Committee on Cognitive Networks Newsletter*, vol. 3, no. 2, pp. 30–34, Nov. 2017.
- [4] A.-A. A. Boulogeorgos, "Interference mitigation techniques in modern wireless communication systems," Ph.D. dissertation, Aristotle University of Thessaloniki, Thessaloniki, Greece, Sep. 2016.
- [5] A.-A. A. Boulogeorgos and A. Alexiou, "Performance analysis of reconfigurable intelligent surface-assisted wireless systems and comparison with relaying," *IEEE Access*, vol. 8, pp. 94463–94483, 2020.

- [6] A.-A. A. Boulogeorgos, A. Alexiou, T. Merkle, C. Schubert, R. Elschner, A. Katsiotis, P. Stavrianos, D. Kritharidis, P. K. Chartsias, J. Kokkonemi, M. Juntti, J. Lehtomäki, A. Teixeira, and F. Rodrigues, "Terahertz technologies to deliver optical network quality of experience in wireless systems beyond 5G," *IEEE Commun. Mag.*, vol. 56, no. 6, pp. 144–151, Jun. 2018.
- [7] E. N. Papatirou, A.-A. A. Boulogeorgos, and A. Alexiou, "Performance analysis of THz wireless systems in the presence of antenna misalignment and phase noise," *IEEE Commun. Lett.*, vol. 24, no. 6, pp. 1211–1215, Jun. 2020.
- [8] J. Kokkonemi, A.-A. A. Boulogeorgos, M. Aminu, J. Lehtomäki, A. Alexiou, and M. Juntti, "Impact of beam misalignment on THz wireless systems," *Nano Commun. Networks*, vol. 24, p. 100302, May 2020.
- [9] E. N. Papatirou, A.-A. A. Boulogeorgos, and A. Alexiou, "Performance evaluation of thz wireless systems under the joint impact of misalignment fading and phase noise," *ArXiv*, Jul. 2019.
- [10] A.-A. A. Boulogeorgos, E. N. Papatirou, and A. Alexiou, "Analytical performance evaluation of THz wireless fiber extenders," in *IEEE 30th Annual International Symposium on Personal, Indoor and Mobile Radio Communications (PIMRC)*. IEEE, Sep. 2019.
- [11] —, "A distance and bandwidth dependent adaptive modulation scheme for THz communications," in *19th IEEE International Workshop on Signal Processing Advances in Wireless Communications (SPAWC)*, Kalamata, Greece, Jul. 2018.
- [12] E. N. Papatirou, J. Kokkonemi, A.-A. A. Boulogeorgos, J. Lehtomäki, A. Alexiou, and M. Juntti, "A new look to 275 to 400 ghz band: Channel model and performance evaluation," in *IEEE International Symposium on Personal, Indoor and Mobile Radio Communications (PIMRC)*, Bolonia, Italy, Sep. 2018.
- [13] A.-A. A. Boulogeorgos, S. Goudos, and A. Alexiou, "Users association in ultra dense THz networks," in *IEEE International Workshop on Signal Processing Advances in Wireless Communications (SPAWC)*, Kalamata, Greece, Jun. 2018.
- [14] G. Stratidakis, A.-A. A. Boulogeorgos, and A. Alexiou, "A cooperative localization-aided tracking algorithm for THz wireless systems," in *IEEE Wireless Communications and Networking Conference (WCNC)*, Marrakech, Morocco, Apr. 2019.
- [15] Q. H. Abbasi, A. A. Nasir, K. Yang, K. A. Qaraqe, and A. Alomainy, "Cooperative in-vivo nano-network communication at terahertz frequencies," *IEEE Access*, vol. 5, pp. 8642–8647, Mar. 2017.
- [16] Z. Rong, M. S. Leeson, and M. D. Higgins, "Relay-assisted nanoscale communication in the thz band," *Micro Nano Letters*, vol. 12, no. 6, pp. 373–376, 2017.
- [17] M. E. P. Monteiro, J. L. Rebelatto, and G. Brante, "On the energy efficiency of relay-assisted in-vivo nano-networks communications," in *15th International Symposium on Wireless Communication Systems (ISWCS)*, Aug 2018, pp. 1–5.
- [18] Q. Xia and J. M. Jornet, "Cross-layer analysis of optimal relaying strategies for terahertz-band communication networks," in *IEEE 13th International Conference on Wireless and Mobile Computing, Networking and Communications (WiMob)*, Oct. 2017, pp. 1–8.
- [19] A.-A. A. Boulogeorgos and A. Alexiou, "Error analysis of mixed THz-RF wireless systems," *IEEE Communications Letters*, pp. 1–1, 2019.
- [20] I. S. Gradshteyn and I. M. Ryzhik, *Table of Integrals, Series, and Products*, 6th ed. New York: Academic, 2000.
- [21] A.-A. A. Boulogeorgos, E. N. Papatirou, and A. Alexiou, "Analytical performance assessment of THz wireless systems," *IEEE Access*, vol. 7, no. 1, pp. 1–18, Jan. 2019.
- [22] J. Kokkonemi, J. Lehtomäki, and M. Juntti, "Simplified molecular absorption loss model for 275-400 gigahertz frequency band," in *12th European Conference on Antennas and Propagation (EuCAP)*, London, UK, Apr. 2018.

